Multimode soliton dynamics in perturbed ladder lattices

Oleksiy O. Vakhnenko[1,2] and Michael J. Velgakis[1]
[1]Engineering Science Department, University of Patras, Patras 26110, Greece
[2]Department of Nonlinear Physics of Condensed Matter, Bogolyubov Institute for Theoretical Physics, Kyïv 03143, Ukraine
(Received 21 March 2000; revised manuscript received 27 July 2000; published 27 December 2000)

We investigate the interplay between the longitudinal and lateral solitonic modes in perturbed ladder lattices in regard to the transmission of soliton wave packet. (1) In a longitudinal uniform field the lateral and longitudinal solitonic modes are shown to be independent. However, unlike in the unperturbed case the dynamics of the soliton center of mass becomes confined within a finite spatial domain via the Bloch-Zener mechanism in the longitudinal direction and due to the transverse finiteness of the ladder in the lateral one. (2) The segment of on-site impurities causes the soliton mode-mode mixing. As a result the soliton exhibits rather complex two- or three-dimensional dynamics accompanied by wave radiation which may give rise to soliton trapping. Nevertheless, under some specific conditions the soliton is able to bypass even the strong impurities slaloming between them. In particular, the slalom soliton dynamics is possible on a ladder lattice with a segment of zigzig-distributed on-site impurities. We formulate the conditions favorable to the case and show that their violation gives rise to either soliton trapping on or soliton reflection from the impure segment. (3) Finally, we study the effect of the modified transverse bond on the longitudinal soliton dynamics and reveal that it might act on the soliton as either an attractive or a repulsive potential, depending on the sign of the transverse energy of the ingoing soliton. The effect is essentially a solitonic one and becomes strictly pronounced for heavy solitons, when imperfection-induced radiation effects are exponentially suppressed. We expect that transverse-bond imperfection could serve as a filter selecting the solitons with prescribed properties. A similar function is feasible for zigzag-distributed on-site impurities too.

DOI: 10.1103/PhysRevE.63.016612 PACS number(s): 45.05.+x, 05.45.Yv, 72.10.Fk

I. INTRODUCTION

Driven by the contemporary boom in the field of optical telecommunications [1] scientific interest in nonlinear Schrödinger and related systems is exhibiting the same rapid growth [2,3]. Except for widely known applications to the problems of light pulse propagation in optical fibers [4,5] the models of nonlinear Schrödinger type serve as a good starting point for the investigation of a number of other physical phenomena such as energy and charge transport in biological macromolecules [6–8], charge-density-wave conductivity in quasi-one-dimensional conductors [9,10], and the dynamics of dark solitons in Bose-Einstein condensates [11] as well as the self-organization in nonlinear wave turbulence [12] and envelope soliton propagation through cylindrical fibers with a nematic liquid cladding [13].

The most famous among the continuous one-dimensional models are the Zakharov-Shabat [14] and Manakov [15] ones. They are exactly integrable, allow precise Hamiltonian formulations [16], and possess well-developed perturbation theories [17–19]. The corresponding discrete versions [20–25] are also integrable. However, apart from a few exceptions their Hamiltonian formulations are either nonstandard or simply unknown. For example the Ablowitz-Ladik model [20] has nonstandard Poisson brackets [26,16]. As a result an application of its perturbation theory [27] to nonintegrable nonlinear Schrödinger models requires some physically motivated precautions [28]. Namely we always have to transform either the Ablowitz-Ladik model or the model under study to the form prescribing the same Poisson brackets to both of them [28]. Only in this case will the amplitudes of both models be of the same meaning and will we manage to obtain the same analytical results either by means of perturbation theory [28] or within the framework of collective variable (trial Lagrangian) approach [28–31].

In this paper we will follow such kinds of reasoning and investigate the peculiarities of the one-soliton dynamics of intramolecular excitations on multileg (in particular, two-leg) ladder lattices subjected to an external linear potential (Sec. III) or one of two types of imperfections typical exclusively of the multileg ladder lattices (Secs. IV and V). We will show, e.g., that on a two-leg ladder lattice the soliton dynamics actually becomes the two-dimensional one and supports some new and even unexpected effects forbidden principally for one-chain lattices.

In order to avoid unnecessary complications inspired by the Peierls-Nabarro potential relief [28], we invoke here the exactly integrable model of nonlinear intramolecular excitations on a multileg ladder lattice [32–34]:

$$\begin{aligned}
i\dot{q}_\alpha(n) + \sum_{\beta=1}^{M} t_{\alpha\beta} q_\beta(n) + [q_\alpha(n+1) + q_\alpha(n-1)] \\
\times\left[1 + \sum_{\beta=1}^{M} q_\beta(n) r_\beta(n)\right] \\
= \sum_{\beta=1}^{M} [q_\alpha(n-1) q_\beta(n) - q_\alpha(n) q_\beta(n-1)] r_\beta(n), \qquad (1)
\end{aligned}$$

$$-i\dot{r}_{\alpha}(n)+\sum_{\beta=1}^{M} r_{\beta}(n)t_{\beta\alpha}+[r_{\alpha}(n+1)+r_{\alpha}(n-1)]\times\left[1+\sum_{\beta=1}^{M} r_{\beta}(n)q_{\beta}(n)\right]=\sum_{\beta=1}^{M}[r_{\alpha}(n+1)r_{\beta}(n)-r_{\alpha}(n)r_{\beta}(n+1)]q_{\beta}(n), \quad (2)$$

appropriately correcting its on-site amplitudes $q_{\alpha}(n)$ and $r_{\alpha}(n)$ and omitting simultaneously some irrelevant and unphysical terms. Here the overdot stands for the derivative with respect to the dimensionless time τ, and the longitudinal numerical coordinate n runs from minus to plus infinity, while the transverse one α runs from 1 to the number of chains (legs), M. The parameters $t_{\alpha\beta}$ describe the interchain linear coupling, while the constants of the intrachain linear coupling, $t_{\parallel}$, are normalized to unity.

By the way, throughout the paper we will deal with dimensionless quantities exclusively. As a consequence quantities labeling the axes of the illustrative figures (Figs. 1–16) are assumed to be dimensionless too.

II. UNPERTURBED PHYSICALLY CORRECTED MODEL

The model (1),(2) conserves the quantity $\Sigma_{n=-\infty}^{\infty}\ln[1+\Sigma_{\alpha=1}^{M}q_{\alpha}(n)r_{\alpha}(n)]$. However, in terms of $q_{\alpha}(n)$ and $r_{\alpha}(n)$ it scarcely resembles the standard expression for the total number of excitations. For this reason we reformulate the original model (1),(2) in terms of corrected amplitudes

$$Q_{\alpha}(n)=q_{\alpha}(n)/E(n), \quad (3)$$

$$R_{\alpha}(n)=r_{\alpha}(n)/E(n), \quad (4)$$

and obtain

$$\begin{aligned}i\dot{Q}_{\alpha}(n)-\partial H_0/\partial R_{\alpha}(n)&=2E(n+1)dE(n)/d\rho(n)\\&\times\sum_{\beta=1}^{M}[Q_{\alpha}(n)Q_{\beta}(n+1)-Q_{\alpha}(n+1)Q_{\beta}(n)]R_{\beta}(n)\\&+2E(n-1)dE(n)/d\rho(n)\\&\times\sum_{\beta=1}^{M}[Q_{\alpha}(n)Q_{\beta}(n-1)-Q_{\alpha}(n-1)Q_{\beta}(n)]R_{\beta}(n)\\&+E(n-1)E(n)\\&\times\sum_{\beta=1}^{M}[Q_{\alpha}(n-1)Q_{\beta}(n)-Q_{\alpha}(n)Q_{\beta}(n-1)]R_{\beta}(n), \quad (5)\end{aligned}$$

$$\begin{aligned}-i\dot{R}_{\alpha}(n)-\partial H_0/\partial Q_{\alpha}(n)&=2E(n+1)dE(n)/d\rho(n)\\&\times\sum_{\beta=1}^{M}[R_{\alpha}(n)R_{\beta}(n+1)-R_{\alpha}(n+1)R_{\beta}(n)]Q_{\beta}(n)\\&+2E(n-1)dE(n)/d\rho(n)\\&\times\sum_{\beta=1}^{M}[R_{\alpha}(n)R_{\beta}(n-1)-R_{\alpha}(n-1)R_{\beta}(n)]Q_{\beta}(n)\\&+E(n+1)E(n)\\&\times\sum_{\beta=1}^{M}[R_{\alpha}(n+1)R_{\beta}(n)-R_{\alpha}(n)R_{\beta}(n+1)]Q_{\beta}(n). \quad (6)\end{aligned}$$

Here

$$\rho(n)=\sum_{\beta=1}^{M}R_{\beta}(n)Q_{\beta}(n), \quad (7)$$

$$E(n)=\sqrt{\frac{\exp[\rho(n)]-1}{\rho(n)}}, \quad (8)$$

$$\begin{aligned}H_0=&-\sum_{\alpha=1}^{M}\sum_{\beta=1}^{M}\sum_{n=-\infty}^{\infty}R_{\alpha}(n)t_{\alpha\beta}Q_{\beta}(n)\\&-\sum_{\alpha=1}^{M}\sum_{n=-\infty}^{\infty}E(n+1)E(n)\\&\times[Q_{\alpha}(n+1)R_{\alpha}(n)+R_{\alpha}(n+1)Q_{\alpha}(n)]. \quad (9)\end{aligned}$$

The resulting model (5)–(9) conserves the quantity $\Sigma_{n=-\infty}^{\infty}\rho(n)$; however, in view of the right-hand-side terms in Eqs. (5) and (6) it does not permit either the reductions $R_{\alpha}(n)=\pm Q_{\alpha}^{*}(n)$ or any Hamiltonian formulation.

We overcome both of these difficulties simply by omitting the just-mentioned right-hand-side terms. As a result we come to the model

$$i\dot{Q}_{\alpha}(n)=\partial H_0/\partial R_{\alpha}(n), \quad (10)$$

$$-i\dot{R}_{\alpha}(n)=\partial H_0/\partial Q_{\alpha}(n). \quad (11)$$

Under any of the reductions $R_{\alpha}(n)=Q_{\alpha}^{*}(n)$ or $R_{\alpha}(n)=-Q_{\alpha}^{*}(n)$ the model (7)–(11) becomes a Hamiltonian one with the Hamiltonian given by H_0 or $-H_0$, respectively. Its Poisson brackets are standard, whereas the amplitudes $Q_{\alpha}^{*}(n)$, $Q_{\alpha}(n)$ acquire the meaning of probability amplitudes relating to the site n,α. The total number of excitations $\Sigma_{\alpha=1}^{M}\Sigma_{n=-\infty}^{\infty}Q_{\alpha}^{*}(n)Q_{\alpha}(n)$ is conserved as expected.

We call the model (7)–(11) the physically corrected model of nonlinear intramolecular excitations on a multileg ladder lattice. Like both of its predecessors (1), (2), and (5)–(9) it sustains the one-soliton solution as well as the multisoliton solutions of factorized type $Q_{\alpha}(n)=b_{\alpha}Q(n)$. This remarkable fact allows us to use the model (7)–(11) as the main (regular) part of realistic physical models dealing with soliton propagation in imperfect ladder lattices as well as in ladder lattices subjected to external fields.

In this paper we restrict ourselves to the reduction $R_{\alpha}(n)=Q_{\alpha}^{*}(n)$ corresponding to an attractive nonlinearity and bright soliton solutions.

III. LISSAJOU'S SOLITON DYNAMICS ON A LADDER LATTICE IN THE PRESENCE OF A SPATIALLY LINEAR POTENTIAL

The lateral degrees of freedom unleashed by the interchain linear couplings ($t_{\alpha\beta}\neq 0,\alpha\neq\beta$) make the soliton dynamics on multileg ladder lattices substantially richer as compared with that of one-leg ladder lattices [27,28,35–37]. This statement is true even for the simplest case of regular multileg ladder models [32–34].

For this reason it is interesting to study the soliton dynamics in a more general case:

$$i\dot{Q}_\alpha(n)=\partial H/\partial R_\alpha(n), \tag{12}$$

$$-i\dot{R}_\alpha(n)=\partial H/\partial Q_\alpha(n), \tag{13}$$

when the model Hamiltonian $H=H_0+U$ consists of regular, Eq. (9), and perturbed,

$$U=\sum_{\alpha=1}^{M}\sum_{\beta=1}^{M}\sum_{n=-\infty}^{\infty}\sum_{m=-\infty}^{\infty}R_\alpha(n)U_{\alpha\beta}(n|\tau|m)Q_\beta(m), \tag{14}$$

parts. Here the potential matrix $U_{\alpha\beta}(n|\tau|m)\equiv U^*_{\beta\alpha}(m|\tau|n)$ will be specified by the lattice imperfections or the external fields, whereas $R_\alpha(n)\equiv Q^*_\alpha(n)$.

We will use the exact dynamical equations (12) and (13) mainly for the numerical integration. However, when the potential U is spatially linear,

$$U_{\alpha\beta}(n|\tau|m)=-\delta_{\alpha\beta}\delta_{nm}m\mathcal{E}(\tau), \tag{15}$$

the model (12)–(14) permits at least some particular exact solutions. For example, seeking the solution in the form of a one-soliton ansatz

$$Q_\alpha(n)=b_\alpha\sqrt{\ln[1+\sinh^2\mu\,\mathrm{sech}^2\mu(n-x)]}\exp(ikn+i\theta), \tag{16}$$

$$b_\alpha\equiv a_\alpha\Big/\sqrt{\sum_{\beta=1}^{M}a^*_\beta a_\beta}, \tag{17}$$

we come to the set of ordinary differential equations

$$\dot{\mu}=0, \tag{18}$$

$$\dot{x}=2\frac{\sinh\mu}{\mu}\sin k, \tag{19}$$

$$\dot{k}=\mathcal{E}(\tau), \tag{20}$$

$$\dot{b}_\alpha=i\sum_{\beta=1}^{M}t_{\alpha\beta}b_\beta, \tag{21}$$

$$\dot{b}^*_\alpha=-i\sum_{\beta=1}^{M}b^*_\beta t_{\beta\alpha}, \tag{22}$$

$$\dot{\theta}=2\cosh\mu\cos k, \tag{23}$$

which can be formally integrated at any temporal modulation of the uniform field $\mathcal{E}(\tau)$.

The equations of motion (19),(20) and (21),(22) are Hamiltonian with respect to two pairs of canonically conjugated collective variables x,k and b_α,b^*_α and describe, respectively, the longitudinal and lateral dynamics of the soliton as a whole.

When the lattice is the two-leg one, $M=2$, $t_{\alpha\beta}=(1-\delta_{\alpha\beta})t$, this dynamics can be readily traced in terms of longitudinal

$$X=\frac{\sum_{n=-\infty}^{\infty}\sum_{\alpha=1}^{2}nR_\alpha(n)Q_\alpha(n)}{\sum_{n=-\infty}^{\infty}\sum_{\alpha=1}^{2}R_\alpha(n)Q_\alpha(n)} \tag{24}$$

and lateral

$$Y=\frac{\sum_{n=-\infty}^{\infty}\sum_{\alpha=1}^{2}(-1)^\alpha R_\alpha(n)Q_\alpha(n)}{\sum_{n=-\infty}^{\infty}\sum_{\alpha=1}^{2}R_\alpha(n)Q_\alpha(n)} \tag{25}$$

coordinates of the nonlinear wave packet. The situation becomes especially simple provided the field $\mathcal{E}(\tau)$ is constant, $\mathcal{E}(\tau)=\mathcal{E}$. Indeed, manipulating the dynamical equations (19)–(22) with the use of X and Y calculated on the one-soliton ansatz (16),(17) we obtain

$$X=\frac{2\sinh\mu}{\mu\mathcal{E}}\{\cos k(0)-\cos[\mathcal{E}\tau+k(0)]\}+x(0), \tag{26}$$

$$Y=-[\cos 2\varphi\cos(2t\tau)+\sin(\delta_1-\delta_2)\sin 2\varphi\sin(2t\tau)], \tag{27}$$

where the identity $X\equiv x$ has been taken into account. The initial conditions for b_1 and b_2 were parametrized as follows: $b_1(0)=\exp(i\delta_1)\cos\varphi$, $b_2(0)=\exp(i\delta_2)\sin\varphi$.

Thus the solitonic center of mass exhibits two independent mutually orthogonal motions along and across the ladder lattice with the cyclic frequencies given by $\omega_\parallel=\mathcal{E}$ and $\omega_\perp=2t$, respectively. The former is nothing but the well-known Bloch-Zener oscillations [38,39] caused by the interplay between the linear potential and the spatial discreteness of the lattice, while the latter is the beating oscillations [32–34] originating from the interchain linear coupling t.

The Bloch oscillations are experimentally observable on semiconductor superlattices (see, e.g., [40] and references therein). They also have been intensively studied within the framework of different one-chain nonlinear Schrödinger models [41–45]. When related to the arrays of optical waveguides, the effects, generally analogous to those of Bloch oscillations and dynamical localization, are also under intense experimental [46] and theoretical [47] study.

The amplitudes of Bloch ($A_\parallel$) and beating ($A_\perp$) oscillations are evidently given by

$$A_\parallel=\frac{2\sinh\mu}{\mu\mathcal{E}}, \tag{28}$$

$$A_\perp=\sqrt{\cos^2 2\varphi+\sin^2(\delta_1-\delta_2)\sin^2 2\varphi}. \tag{29}$$

At $\mathcal{E}\neq 0$ and $\cos 2\varphi\neq 0$ or/and $\sin(\delta_1-\delta_2)\neq 0$ both of them are finite and nonzero. As a result the parametrically defined trajectory of the soliton center of mass (26),(27) becomes

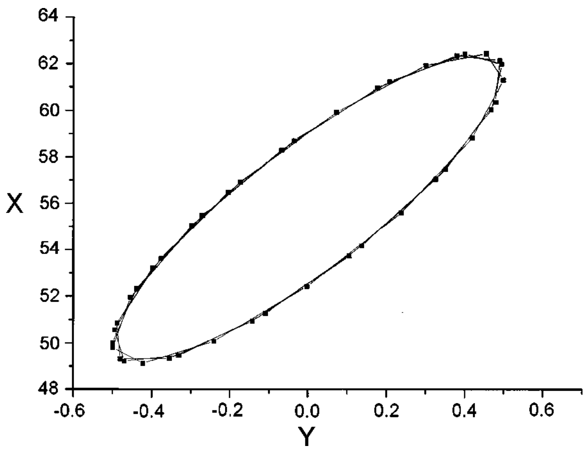

FIG. 1. The trajectory of the soliton center of mass on a ladder lattice in longitudinal uniform field $\mathcal{E}=1$ at $t=1/2$.

confined dynamically within a finite rectangle of length $2A_\parallel$ and width $2A_\perp$. When the periods of longitudinal $T_\parallel = 2\pi/\mathcal{E}$ and lateral $T_\perp = \pi/t$ oscillations become commensurate, $T_\perp/T_\parallel = p/q$ (where p and q are the natural numbers), the soliton c.m. trajectory has to be closed into some of Lissajou's curves (see, e.g., the classical monograph by Hemholtz [48]).

Figures 1 and 2 illustrate typical Lissajou's curves obtained by direct numerical integration of the exact dynamical equations (12)–(15) with the use of definitions (24) and (25) for the coordinates of the solitonic center of mass. Parameters irrelevant to the frequencies of longitudinal and lateral oscillations were kept the same for both of these pictures. Namely, we choose $k(0)=\pi/6$, $x(0)=50$, $\mu=3$, $\varphi=\pi/6$, and $\delta_2-\delta_1=\pi$. However, the strength of the longitudinal uniform field $\mathcal{E}$ and the strength of the interchain linear coupling t were taken to be different. In particular $\mathcal{E}=1, t=1/2$ for Fig. 1 and $\mathcal{E}=3$, $t=1$ for Fig. 2. Hence the ratio $T_\perp/T_\parallel$ is equal to 1 and 3/2 for Fig. 1 and Fig. 2 respectively.

We would like to stress that the trajectories of the soliton center of mass have been calculated with great accuracy everywhere throughout the paper. The reason for the interpolation of trajectories by straight segments is only to mark the points equally distanced in time.

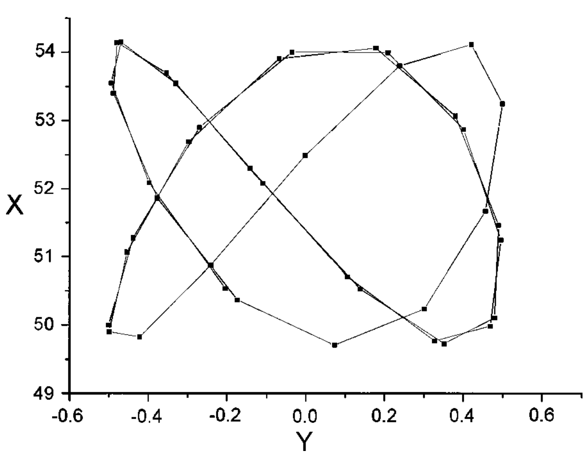

FIG. 2. The trajectory of the soliton center of mass on a ladder lattice in longitudinal uniform field $\mathcal{E}=3$ at $t=1$.

IV. TWO-DIMENSIONAL SOLITON DYNAMICS ON A LADDER LATTICE WITH ZIGZAG-DISTRIBUTED IMPURITIES

In this section we demonstrate the advantages of the two-dimensional soliton dynamics on a ladder lattice in bypassing strong on-site impurities as compared to one-chain lattices [36,42,49], where the two-dimensional dynamics is forbidden.

We take the impurity potential matrix to be in the form

$$U_{\alpha\beta}(n|\tau|m)=\delta_{\alpha\beta}\delta_{nm}V_\beta(m)\sum_{s=0}^{Z-1}\Delta(m-n_\beta-Mls), \tag{30}$$

where $V_\alpha(n_\alpha+Mls)$ is the energy shift of the impurity molecule located on the αth chain within the $(n_\alpha+Mls)$th unit cell and n_α is the position of the first impurity on the αth chain. The integer Ml measures the distance between the impurities belonging to the same chain, and Z is the total number of impurities on each chain, whereas $\Delta(n-m)$ is the Kronecker delta function δ_{nm}. In a particular case, $n_\alpha=n_i+(\alpha-1)l$, $\alpha=1,2,\ldots,M$, for $M=2$, the impurity matrix (30) corresponds to the zigzag distribution of impurities on a two-leg ladder lattice, while for $M=3$ it describes the spiral distribution of impurities on a three-leg ladder lattice.

We consider in detail only the case of zigzag impurity distribution on a two-leg ladder lattice ($n_1=n_i, n_2=n_i+l$, $M=2$) and we examine some different scenarios of soliton propagation through the impure segment. Nevertheless, some initial formulas, in particular Eqs. (31)–(34), will be written in a general form to be equally applicable to the three-leg ladder lattice with a spiral distribution of impurities.

We start with a qualitative estimation of soliton dynamics within the framework of the collective coordinate approach [28–31] in the lowest approximation. Substituting the one-soliton ansatz (16),(17) into the model Lagrangian

$$L=\frac{i}{2}\sum_{\alpha=1}^{M}\sum_{n=-\infty}^{\infty}[R_\alpha(n)\dot{Q}_\alpha(n)-\dot{R}_\alpha(n)Q_\alpha(n)]-H \tag{31}$$

and using the standard Euler-Lagrange formalism with respect to the collective variables $(x,k,a_\alpha,a_\alpha^*,\mu,\theta)$, we obtain the following set of dynamical equations:

$$\dot{x}=\partial\mathcal{H}/\partial k, \quad \dot{k}=-\partial\mathcal{H}/\partial x, \tag{32}$$

$$i\dot{b}_\alpha=\partial\mathcal{H}/\partial b_\alpha^*, \quad -i\dot{b}_\alpha^*=\partial\mathcal{H}/\partial b_\alpha. \tag{33}$$

Here

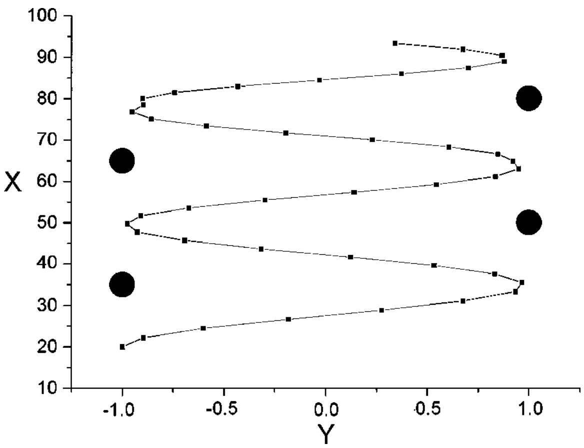

FIG. 3. The trajectory of the soliton center of mass on a ladder lattice with the attractive on-site impurities $V=-10$ for $k(0)=0.7965$ and $\varphi=0$.

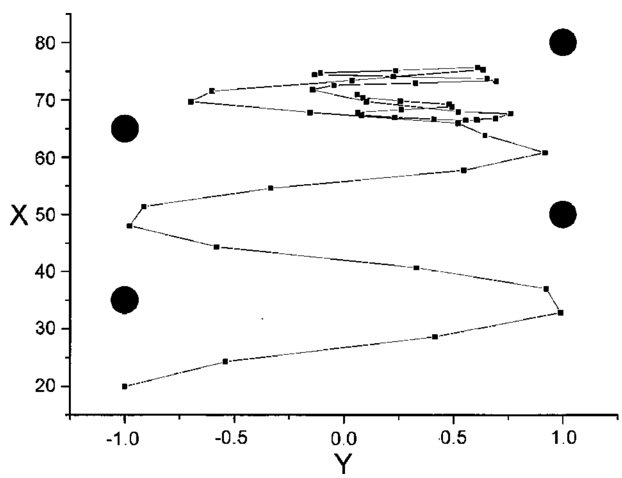

FIG. 5. The trajectory of the soliton center of mass on a ladder lattice with the attractive on-site impurities $V=-10$ for $k(0)=0.7$ and $\varphi=0$.

$$\mathcal{H}=-\frac{2\sinh\mu}{\mu}\cos k-\sum_{\alpha=1}^{M}\sum_{\beta=1}^{M}b_\alpha^* t_{\alpha\beta}b_\beta+\frac{V}{2\mu}\sum_{\alpha=1}^{M}b_\alpha^* b_\alpha \times\sum_{s=1}^{Z-1}\ln\{1+\sinh^2\mu\,\mathrm{sech}^2\mu[x-n_i(\alpha-1)l-Mls]\} \tag{34}$$

is an effective Hamiltonian with the pairs x,k and b_α,b_α^* to be canonically conjugated variables, where for simplification reasons we have considered all impurities to be of the same strength, $V_\alpha[n_i+(\alpha-1)l+Mls]\equiv V$. The parameter μ is understood to be positive and time independent, $\dot{\mu}=0$. Its relation to the longitudinal width of the soliton d is estimated as $d\sim\coth\mu$.

As in the case of the linear external potential the variables x and k have a sense of the mean longitudinal coordinate of the soliton pattern and corresponding momentum, whereas the variables b_α and b_α^* reproduce the temporal redistribution of the soliton density along the lateral direction.

Of course we also could take into account the principal possibility of the longitudinal soliton breathing multiplying the trial soliton function (16),(17) by the factor $\sqrt{\nu/\mu}\exp[icf(n-x)]$ with $f(-y)=f(y)$. However, unlike in continuous models [50,51] or discrete models dealing with immobile pulses [52], in our problem such a kind of generalization seems to be of minor practical validity since the corresponding trial Lagrangian can scarcely be calculated with an acceptable accuracy.

In a regular ladder lattice ($V=0$) with $t_{\alpha\beta}=(1-\delta_{\alpha\beta})t$ the equations of the collective dynamics (32)–(34) are exact. As a result the lateral (25) and longitudinal (24) mean coordinates of the soliton pattern are governed by the equation of the harmonic oscillator, $\ddot{Y}+(2t)^2Y=0$, and the equation of uniform motion, $\ddot{X}=0$, respectively. These equations give rise to a sinusoidal trajectory for the soliton center of mass.

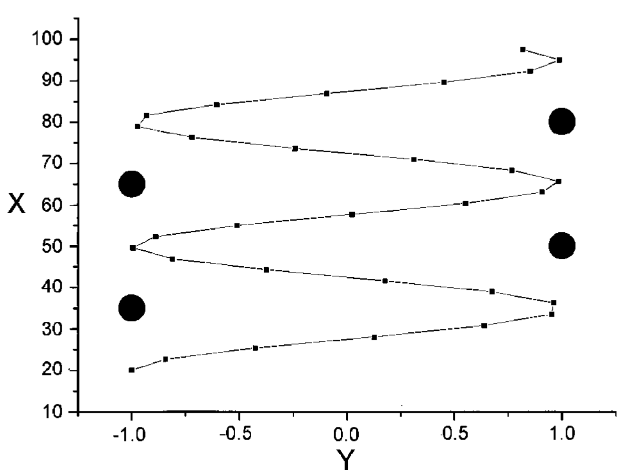

FIG. 4. The trajectory of the soliton center of mass on a ladder lattice with the repulsive on-site impurities $V=+10$ for $k(0)=0.7965$ and $\varphi=0$.

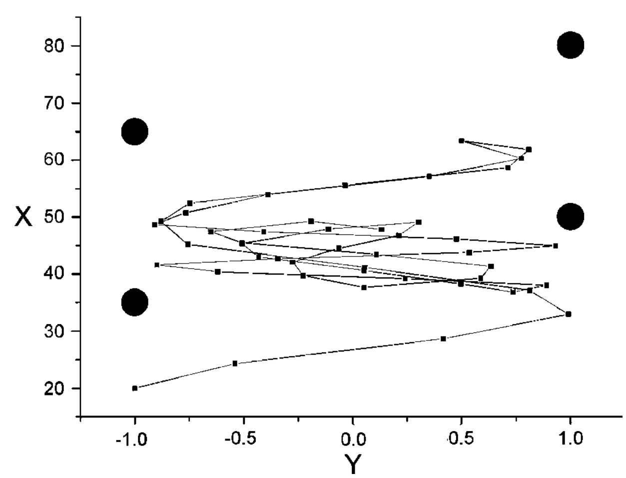

FIG. 6. The trajectory of the soliton center of mass on a ladder lattice with the repulsive on-site impurities $V=+10$ for $k(0)=0.7$ and $\varphi=0$.

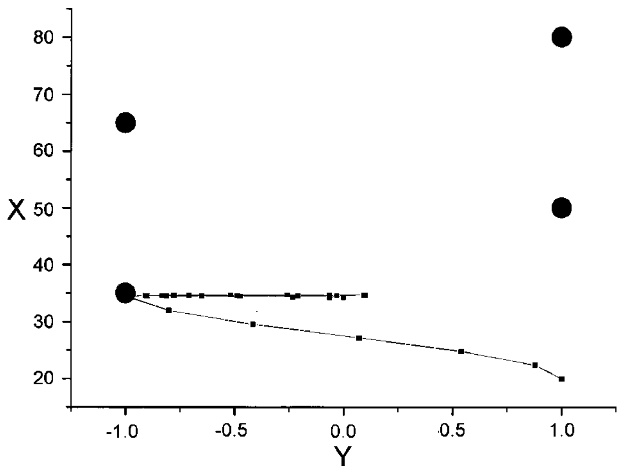

FIG. 7. The trajectory of the soliton center of mass on a ladder lattice with the attractive on-site impurities $V=-10$ for $k(0)=0.7965$ and $\varphi=\pi/2$.

The amplitude of the sinusoidal trajectory coincides with the amplitude of the beating oscillations $A_{\perp}$ given by Eq. (29) and can vary from zero to unity, depending on the initial conditions of the transverse solitonic distribution $b_1(0)=\exp(i\delta_1)\cos\varphi$, $b_2(0)=\exp(i\delta_2)\sin\varphi$.

In an irregular ladder lattice ($V\neq 0$) the equations of the collective dynamics (32)–(34) are approximate. They are certainly valid when the impurity-induced effects of wave radiation [53] and the soliton-induced effects of the impurity excitation [54] are small. For an isolated impurity $Z=1$, $V_{\alpha}(n_{\alpha}+Mls)=V\delta_{\alpha 1}$, these effects are suppressed exponentially, when the radius of the unexcited localized (staggered localized) impurity state $1/\gamma$ exceeds the longitudinal width of the soliton d. Here $\gamma=|\mathrm{arsh}(V/2)|$. The requirement $\gamma^{-1}>d$ is a rather strong condition. It justifies the adiabatic theory (32)–(34) at any stage of the one-soliton dynamics. Moreover, it preserves the soliton robustness against the impurity-induced two-soliton splitting, at least in processes of soliton-impurity scattering [55].

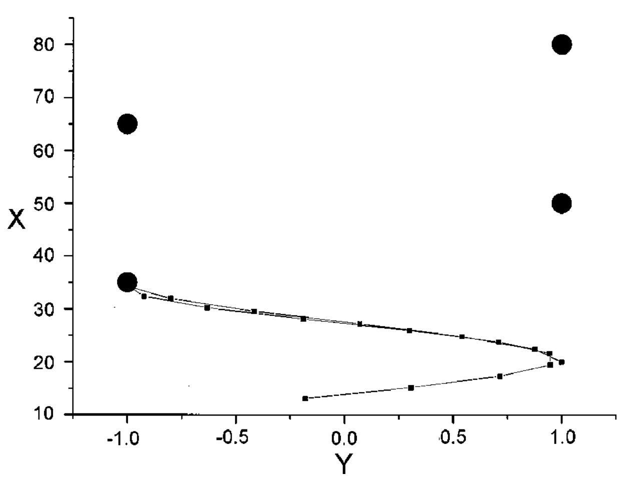

FIG. 8. The trajectory of the soliton center of mass on a ladder lattice with the repulsive on-site impurities $V=+10$ for $k(0)=0.7965$ and $\varphi=\pi/2$.

In one-chain nonlinear systems the restriction $\gamma^{-1}>d$ is a decisive condition although it undoubtedly could be ignored at the early and some final stages of the soliton-impurity scattering, when the distance between soliton and impurity exceeds substantially the soliton width.

On the contrary, in two-chain ladder nonlinear systems, the restriction $\gamma^{-1}>d$ can be relaxed or even neglected in cases when the soliton and impurity are located on opposite chains, irrespectively to the longitudinal distance between them. In particular, according to the equations of collective dynamics (32)–(34) we can expect a very weak disturbance of the sinusoidal soliton trajectory with unity amplitude by a finite segment of strong impurities $\gamma^{-1}<d$ zigzag distributed in antiphase order to the ideal sinusoidal soliton trajectory. As a consequence, the soliton is bypassed in a slalom motion between the obstacles, resulting in practically full soliton transmission through the impure segment.

More precisely, under the assumption of zero longitudinal solitonic width, the basic condition supporting the soliton slalom reads as

$$l=\left(j+\frac{1}{2}\right)T_{\perp}v_{\parallel}, \quad j=0,1,2,\ldots, \tag{35}$$

where $T_{\perp}=\pi/t$ and $v_{\parallel}=(2/\mu)\sinh\mu\,\sin k(0)$ are the period of lateral soliton oscillations and the longitudinal soliton velocity in an ideal ladder lattice, respectively. This condition synchronizes the longitudinal and lateral soliton motion into the slalom motion, provided the ideal soliton trajectory is passed through the lattice site $n=n_i,\alpha=2$ situated just across from the first impurity site $n=n_i,\alpha=1$.

In real cases, the above requirements must be supplemented by a natural demand of the soliton narrowness in the longitudinal direction:

$$d\ll\frac{1}{2}T_{\perp}v_{\parallel}. \tag{36}$$

We have verified the qualitative results of the adiabatic theory by solving numerically the exact dynamical equations (12),(13) with the perturbed part of Hamiltonian (14) specified by Eq. (30) and $V_{\alpha}(n_{\alpha}+Mls)\equiv V$, $n_{\alpha}=n_i+(\alpha-1)l$, $M=2$, $Z=2$. In other words, we have considered the soliton propagation on a two-leg ladder lattice with four zigzag-distributed on-site impurities.

In our calculations both impurity types, attractive ($V<0$) and repulsive ($V>0$), have been inspected. The longitudinal distance between neighboring impurities has been fixed at $l=15$. To make the comparison more clear, we kept the profile of ingoing solitons to be the same ($\mu=3$) for all cases (see Figs. 3–8). Also, the initial solitons were implanted on the same unit cell $X(0)=n_0\equiv 20$ at a fixed distance $n_i-n_0=15$ from the first impurity. The intrachain and interchain coupling constants were kept at the values $t_{\parallel}=1$ and $t=1/2$, respectively. Finally, we kept fixed the difference $\delta_2-\delta_1=\pi$. However, the initial soliton velocity $(2/\mu)\sinh\mu\,\sin k(0)$ and the parameter φ, which determine both the initial amplitude of lateral soliton oscillations (29) and the initial transverse position of the soliton center of mass $Y(0) = -\cos 2\varphi$, can be varied.

We have presented our numerical results using Eqs. (24) and (25) as definitions of the longitudinal and lateral coordinates of any nonlinear pulselike wave packet regardless of the particular analytical ansatz (16),(17).

All odd-numbered figures (i.e., Figs. 3, 5, and 7) represent the soliton trajectory through a ladder lattice with an attractive impurity interaction $V = -10$, while the even-numbered figures (Figs. 4, 6, and 8) are related to the repulsive impurity interaction $V = +10$.

Figures 3 and 4 are referred to the situation when the synchronization conditions are satisfied. That is, $j = 0$ [in Eq. (35)], $k(0) = 0.7965$, and $\varphi = 0$. We clearly see that the soliton slaloms between the impurities (marked by large solid circles) and finally it escapes from the impure segment. Consequently the soliton is fully transmitted through the impure segment.

However, when the initial soliton momentum is slightly decreased, $k(0) = 0.7$, we observe a soliton trapping in the impure segment, irrespectively of the sign of the soliton-impurity interaction (Figs. 5 and 6). Naturally, the soliton trapping is caused by radiation effects of low-amplitude waves.

In Figs. 7 and 8 the synchronization conditions are violated by assigning the initial soliton on chain 2 instead of 1, contrary to the case of Figs. 3 and 4. Specifically, we took $k(0) = 0.7965$ and $\varphi = \pi/2$. In this case, the soliton approaching the first impurity is trapped or reflected by it, for an attractive $V = -10$ or repulsive $V = +10$ interaction, respectively.

As a result, the dynamics of soliton propagation on an impure ladder lattice with zigzag-distributed impurities is shown to be rather complex and rich. Depending on the soliton initial conditions and the sign of the soliton-impurity interaction, we can observe (a) a slalom soliton motion, leading practically to the soliton transmission through the impure segment, (b) soliton trapping in the impure segment, accompanied by the radiation of spatially extended waves, and (c) soliton reflection from the impure segment.

V. ATTRACTIVE-REPULSIVE ALTERNATIVE IN A SOLITON INTERACTION WITH MODIFIED TRANSVERSE BONDS

Another sort of defect feasible for the multileg ladder lattices is the local modification of transverse bonds:

$$U_{\alpha\beta}(n|\tau|m) = -\Delta(n-n_t)\Delta(m-n_t)h_{\alpha\beta}. \tag{37}$$

Here the parameters $h_{\alpha\beta}$ describe the changes of lateral coupling parameters $t_{\alpha\beta}$ within the (n_t)th unit cell.

In what follows we consider only the case of proportional modification,

$$h_{\alpha\beta} = w t_{\alpha\beta}, \tag{38}$$

bearing in mind that it is always justified at least for the two-leg ladder lattice. We will see that such a kind of modification might act on the longitudinal soliton dynamics in two absolutely different ways: either as a repulsive or as an attractive potential depending exclusively on the purely intrinsic conditions of the transverse solitonic modes. The main features of this effect can be understood already within the framework of the trial Lagrangian formalism.

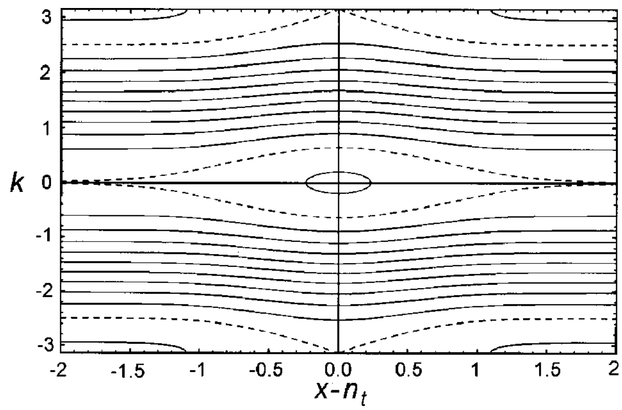

FIG. 9. A phase portrait of longitudinal soliton motion on a ladder lattice with the modified transverse bond for the attractive case $w\eta > 0$, $\mathcal{H}(\pm\pi, n_t) > \mathcal{H}(0, n_t \pm \infty)$. $wt = 2$, $\delta_2 - \delta_1 = 0$, and $\varphi = \pi/6$.

As in the previous section we substitute the one-soliton ansatz (16),(17) into the Lagrangian (31) with the perturbation (14) specified by Eqs. (37) and (38) and once again apply the Euler-Lagrange formalism. As a result we obtain the dynamical equations for the collective variables x, k and b_α, b_α^* in the same Hamiltonian form (32),(33) with $\dot{\mu} = 0$. However, the explicit expression for the effective Hamiltonian $\mathcal{H}$ has to be changed and reads as

$$\mathcal{H} = -\frac{2\sinh\mu}{\mu}\cos k - \eta - \frac{w\eta}{2\mu} \times \ln[1 + \sinh^2\mu\,\mathrm{sech}^2\mu(x-n_t)], \tag{39}$$

where

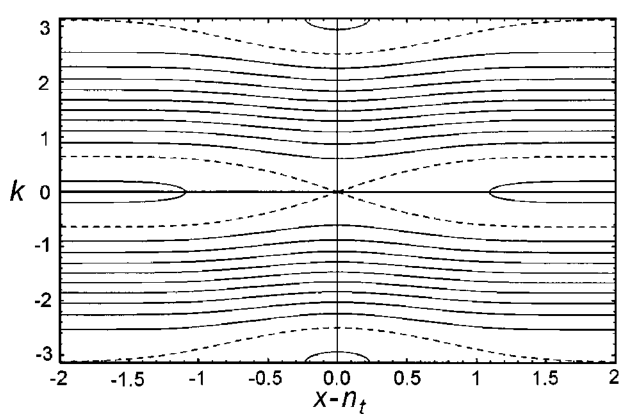

FIG. 10. A phase portrait of longitudinal soliton motion on a ladder lattice with the modified transverse bond for the repulsive case $w\eta < 0, \mathcal{H}(0, n_t) < \mathcal{H}(\pm\pi, n_t \pm \infty)$. $wt = 2$, $\delta_2 - \delta_1 = \pi$, and $\varphi = \pi/6$.

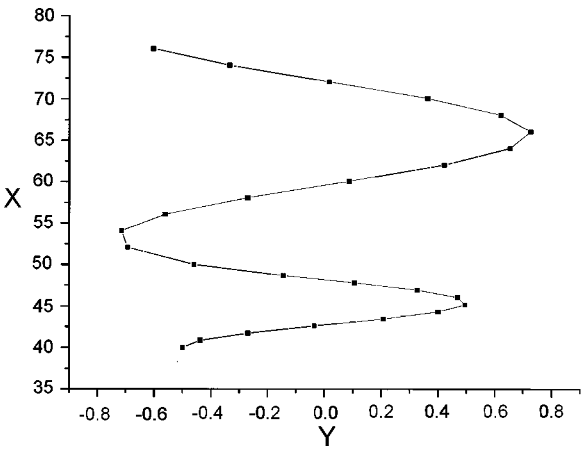

FIG. 11. The trajectory of the soliton center of mass on a ladder lattice with the modified transverse bond $wt=2$ $(w=4,t=1/2)$ for $k(0)=\pi/12$, $\delta_2-\delta_1=0$, and $\varphi=\pi/6$.

$$\eta \equiv \sum_{\alpha=1}^{M} \sum_{\beta=1}^{M} b_\alpha^* t_{\alpha\beta} b_\beta . \tag{40}$$

The quantity η when being conserved appears to be of key importance in the whole problem under study. Its conservation is possible provided the transverse coupling parameters $t_{\alpha\beta}$ are time independent. Indeed, differentiating the definition (40) with respect to time τ and subsequently using the dynamical equations for b_α and b_α^*, Eqs. (33), (39), and (40), yields $\dot{\eta}\equiv 0$. As a result the effective equations of the longitudinal dynamics, Eqs. (32),(39), become self-consistent, insofar as the effect of the transverse subsystem is taken into account integrally by means of the conserved quantity η. Of course, we can safely calculate η at any fixed moment of time including the initial one. Hence the value and sign of this quantity are regulated by the initial conditions of the transverse solitonic modes. For example, turning to the two-chain ladder model $M=2$, $t_{\alpha\beta}=(1-\delta_{\alpha\beta})t$ and using the parametrization $b_1(0)=\exp(i\delta_1)\cos\varphi$, $b_2(0)=\exp(i\delta_2)\sin\varphi$, we come to the expression

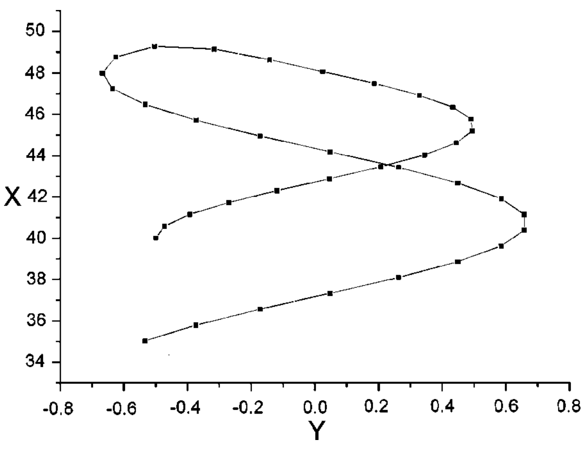

FIG. 12. The trajectory of the soliton center of mass on a ladder lattice with the the modified transverse bond $wt=2$ $(w=4,t=1/2)$ for $k(0)=\pi/12$, $\delta_2-\delta_1=\pi$, and $\varphi=\pi/6$.

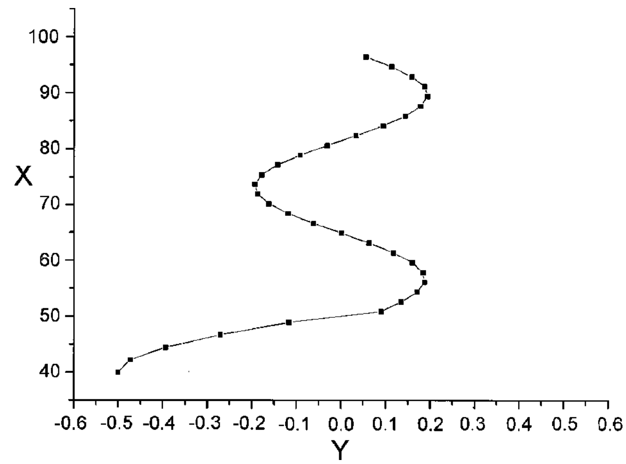

FIG. 13. The trajectory of the soliton center of mass on a ladder lattice with the modified transverse bond $wt=2$ $(w=4,t=1/2)$ for $k(0)=\pi/2$, $\delta_2-\delta_1=0$, and $\varphi=\pi/6$.

$$\eta = t\cos(\delta_1-\delta_2)\sin 2\varphi, \tag{41}$$

which confirms the above statement.

From Eq. (39) we see that except for other factors the sign and strength of the effective longitudinal potential energy are determined by those of η. Thus we could treat η as some effective charge of the soliton. Through the effective charge η we are capable of regulating the character of the interaction between the soliton and the modified transverse bond from attractive to repulsive and vice versa by merely variating the initial parameters of the transverse soliton distribution. We believe this effect might play a crucial role in the phenomena of soliton separation or selection with respect to the effective transverse energy of the ingoing soliton $-\eta$, which happens to be determined by the effective soliton charge η.

Similarly to the previous section the qualitative theory of this section is certainly valid provided the imperfection-induced effects of wave radiation by soliton and soliton-

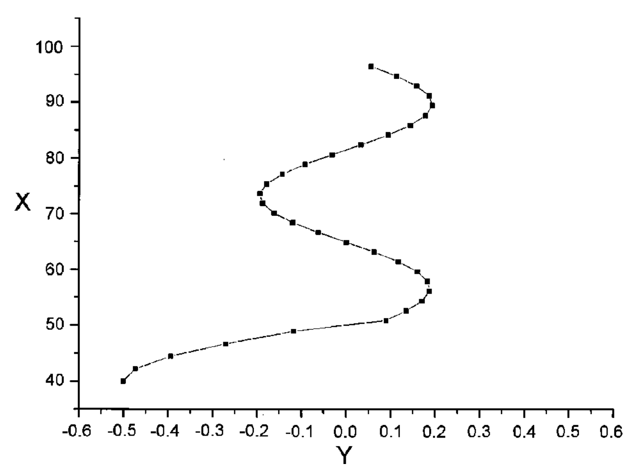

FIG. 14. The trajectory of the soliton center of mass on a ladder lattice with the modified transverse bond $wt=2$ $(w=4,t=1/2)$ for $k(0)=\pi/2$, $\delta_2-\delta_1=\pi$, and $\varphi=\pi/6$.

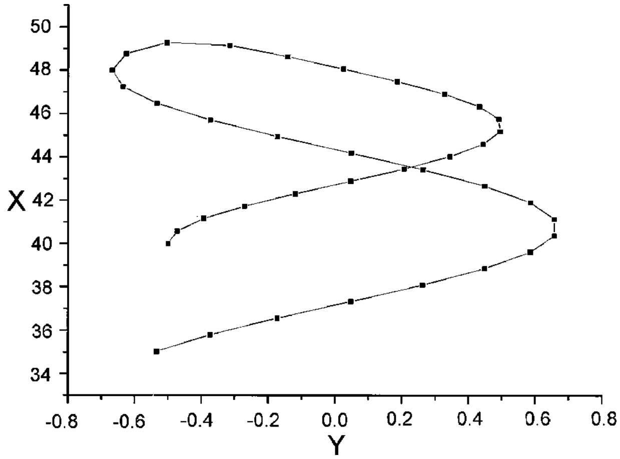

FIG. 15. The trajectory of the soliton center of mass on a ladder lattice with the the modified transverse bond $wt=2$ $(w=4,t=1/2)$ for $k(0)=11\pi/12$, $\delta_2-\delta_1=0$, and $\varphi=\pi/6$.

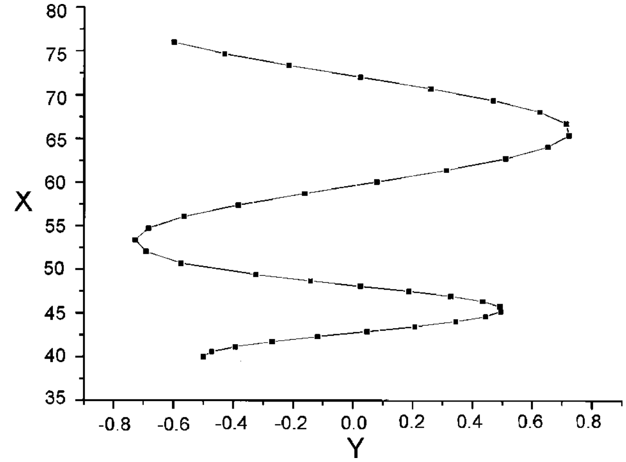

FIG. 16. The trajectory of the soliton center of mass on a ladder lattice with the modified transverse bond $wt=2$ $(w=4,t=1/2)$ for $k(0)=11\pi/12$, $\delta_2-\delta_1=\pi$, and $\varphi=\pi/6$.

induced effects of impurity-state excitation are negligible. For the modified transverse bond on a two-leg ladder lattice, e.g., these effects are small when the radius of the corresponding unexcited localized (staggered localized) state $1/\Gamma$ exceeds the longitudinal width of the soliton d. Here $\Gamma=|\mathrm{arsh}(wt/2)|$. However, unlike in the case of on-site impurities, the restriction $\Gamma^{-1}>d$ cannot be relaxed since the transverse-bond imperfection is stretched equally to both the chains. Here it is worth noticing that in practice the restriction $\Gamma^{-1}>d$ can be readily replaced by the approximate but more simple one

$$2\tanh\mu>|wt|. \tag{42}$$

Proceeding further we can find possible regimes of longitudinal soliton motion analyzing the family of phase trajectories $\mathcal{H}(k,x)=E$ parametrized by the effective energy E. (The points $k=-\pi$ and $k=\pi$ should be considered as identical.)

Thus when the interaction between soliton and transverse imperfection is attractive $w\eta>0$ the two types of phase portraits are feasible depending on the relationships between $\mathcal{H}(\pm\pi,n_t)$ and $\mathcal{H}(0,n_t\pm\infty)$. However, the basic restriction (42) selects only the type with $\mathcal{H}(\pm\pi,n_t)>\mathcal{H}(0,n_t\pm\infty)$ [i.e., $4\sinh\mu>w\eta\ln(\cosh\mu)$]. The typical phase portrait related to the case when $\mathcal{H}(\pm\pi,n_t)>\mathcal{H}(0,n_t\pm\infty)$ is plotted in Fig. 9, where $\mu=3$, $wt=2$, $\delta_2-\delta_1=0$, and $\varphi=\pi/6$. The three different regimes of soliton motion are as follows: (i) oscillations near the bottom of the Hamiltonian surface $x=n_t$, $k=0$ at $\mathcal{H}(0,n_t)<E<\mathcal{H}(0,n_t\pm\infty)$, (ii) open (transport) trajectories at $\mathcal{H}(0,n_t\pm\infty)<E<\mathcal{H}(\pm\pi,n_t)$, and (iii) boomerang trajectories near the line $|k|=\pi$ at $\mathcal{H}(\pm\pi,n_t)<E<\mathcal{H}(\pm\pi,n_t\pm\infty)$.

When the interaction between the soliton and transverse imperfection is repulsive $w\eta<0$ another two types of phase portraits are feasible depending on whether $\mathcal{H}(0,n_t)$ is larger or smaller than $\mathcal{H}(\pm\pi,n_t\pm\infty)$. However, once again the basic restriction (42) selects only one of them, namely, with $\mathcal{H}(0,n_t)<\mathcal{H}(\pm\pi,n_t\pm\infty)$ [i.e., $4\sinh\mu>-w\eta\ln(\cosh\mu)$]. The typical phase diagram related to the case when $\mathcal{H}(0,n_t)<\mathcal{H}(\pm\pi,n_t\pm\infty)$ is plotted in Fig. 10, where $\mu=3$, $wt=2$, $\delta_2-\delta_1=\pi$, and $\varphi=\pi/6$. We clearly see (i) oscillations on the top of Hamiltonian surface $x=n_t$, $|k|=\pi$ at $\mathcal{H}(\pm\pi,n_t\pm\infty)<E<\mathcal{H}(\pm\pi,n_t)$, (ii) open (transport) trajectories at $\mathcal{H}(0,n_t)<E<\mathcal{H}(\pm\pi,n_t\pm\infty)$, and (iii) boomeranglike trajectories near the line $k=0$ at $\mathcal{H}(0,n_t\pm\infty)<E<\mathcal{H}(0,n_t)$.

The described phase diagrams provide a good opportunity for the direct numerical cross-examination of the whole qualitative soliton dynamics formulated in the framework of the pseudocharge concept. We have inspected the exact soliton dynamics with several initial conditions relating to both attractive and repulsive interactions between the soliton and modified transverse bond in the case of a two-leg ladder lattice $M=2$, $t_{\alpha\beta}=(1-\delta_{\alpha\beta})t$ and obtained good agreement with the results of qualitative soliton dynamics.

The results of our calculations were based upon the exact dynamical equations (12) and (13) with the Hamiltonian $H=H_0+U$ specified by the expressions (9),(14) and (37),(38). They are presented in Figs. 11–16 in the form of trajectories of the solitonic center of mass. For comparative reasons with the collective variable theory we took the parameters $\mu=3, wt=2$ $(w=4,\ t=1/2)$, $t_{\parallel}=1$, and $\varphi=\pi/6$ to be the same as in Figs. 9 and 10 for all cases. For the same reasons we kept $\delta_2-\delta_1=0$ for the odd-numbered figures (i.e., Figs. 11, 13, and 15) and $\delta_2-\delta_1=\pi$ for the even-numbered ones (i.e., Figs. 12, 14, and 16). Also the ingoing solitons were implanted on the same unit cell $X(0)=n_0\equiv 40$ at a fixed distance $n_t-n_0=10$ from the modified transverse bond.

Now tracing the ingoing soliton momentum $k(0)$ we see that the odd-numbered figures (i.e., Figs. 11, 13, and 15) are in agreement with the phase portrait described in Fig. 9, while the even-numbered figures (i.e., Figs. 12, 14, and 16) are in agreement with the phase portrait described in Fig. 10. Indeed $k(0)=\pi/12$ is related to the open phase trajectory in

Fig. 9 and the soliton transmission in Fig. 11 at $\delta_2-\delta_1=0$ on the one hand and to the boomerang phase trajectory in Fig. 10 and the soliton reflection in Fig. 12 at $\delta_2-\delta_1=\pi$ on the other. Conversely $k(0)=11\pi/12$ is related to the boomerang phase trajectory in Fig. 9 and the soliton reflection in Fig. 15 at $\delta_2-\delta_1=0$ on the one hand and to the open phase trajectory in Fig. 10 and the soliton transmission in Fig. 16 at $\delta_2-\delta_1=\pi$ on the other. But it is precisely what we expected since apart from other common parameters Figs. 9, 11, 13, and 15 are characterized by the same positive product $w\eta \equiv wt\cos(\delta_1-\delta_2)\sin 2\varphi=\sqrt{3}$. A similar conclusion is valid for Figs. 10, 12, 14, and 16, however with the same negative product $w\eta\equiv wt\cos(\delta_1-\delta_2)\sin 2\varphi=-\sqrt{3}$.

To be sure in the theory of collective soliton dynamics we have changed the sign of the parameter w from positive to negative and performed exact numerical calculations once again. As in the previous case the analytical results have totally been confirmed by direct numerical integration. We do not present here the corresponding pictures only for the sake of brevity.

VI. CONCLUDING REMARKS

In conclusion, we have developed a physically corrected model of intramolecular excitations on a multileg ladder lattice supporting both exact soliton solutions and the standard Hamiltonian formulation. We have subjected this system subsequently to three different perturbations and have investigated the corresponding multimode soliton dynamics. In particular we have paid attention to the uniform longitudinal field, zigzag-distributed on-site impurities, and local modification of transverse bonds and described the effects caused by the nontrivial mixing between the lateral and longitudinal solitonic modes. Most of these effects are summarized in the abstract.

ACKNOWLEDGMENTS

This work was supported in part by the Research Commission, University of Patras, Grant C. Caratheodory 1911/98, and by the INTAS Foundation under Grant No. INTAS 96-0158.

[1] J.-M. Beaufils, Opt. Fiber Technol.: Mater., Devices Syst. **6**, 15 (2000).

[2] Yu. S. Kivshar and B. Luther-Davies, Phys. Rep. **298**, 81 (1998).

[3] Yu. S. Kivshar and D. E. Pelinovsky, Phys. Rep. **331**, 117 (2000).

[4] G. P. Agrawal, *Nonlinear Fiber Optics* (Academic, New York, 1989).

[5] A. Hasegawa, *Optical Solitons in Fibers* (Springer-Verlag, Berlin, 1989).

[6] A. S. Davydov, *Solitons in Molecular Systems* (Kluwer Academic, Dordrecht, 1991).

[7] Z. Ivić, Physica D **113**, 218 (1998).

[8] D. Hennig, Phys. Rev. E **61**, 4550 (2000).

[9] A. A. Eremko, Phys. Rev. B **46**, 3721 (1992).

[10] A. A. Eremko, Phys. Rev. B **50**, 5160 (1994).

[11] X.-J. Chen, J.-Q. Zhang, and H.-Ch. Wong, Phys. Lett. A **268**, 306 (2000).

[12] R. Jordan and Ch. Josserand, Phys. Rev. E **61**, 1527 (2000).

[13] J. A. Reyes and R. F. Rodríguez, Physica D **141**, 333 (2000).

[14] V. E. Zakharov and A. B. Shabat, Zh. Eksp. Teor. Fiz. **61**, 118 (1971) [Sov. Phys. JETP **34**, 62 (1972)].

[15] S. V. Manakov, Zh. Eksp. Teor. Fiz. **65**, 505 (1973) [Sov. Phys. JETP **38**, 248 (1974)].

[16] L. A. Takhtajan and L. D. Faddeev, *Hamil'tonov Podkhod v Teorii Solitonov* (Nauka, Moscow, 1986) [L. D. Faddeev and L. A. Takhtajan, *Hamiltonian Methods in the Theory of Solitons* (Springer, Berlin, 1987)].

[17] D. J. Kaup, SIAM (Soc. Ind. Appl. Math.) J. Appl. Math. **31**, 121 (1976).

[18] V. I. Karpman and E. M. Maslov, Zh. Eksp. Teor. Fiz. **73**, 537 (1977) [Sov. Phys. JETP **46**, 281 (1977)].

[19] T. I. Lakoba and D. J. Kaup, Phys. Rev. E **56**, 6147 (1997).

[20] M. J. Ablowitz and J. F. Ladik, J. Math. Phys. **17**, 1011 (1976).

[21] A. G. Izergin and V. E. Korepin, Dokl. Akad. Nauk SSSR **259**, 76 (1981) [Sov. Phys. Dokl. **26**, 653 (1981)].

[22] E. Date, M. Jimbo, and T. Miwa, J. Phys. Soc. Jpn. **52**, 761 (1983).

[23] G. R. W. Quispel, F. W. Nijhoff, H. W. Capel, and J. van der Linden, Physica A **125**, 344 (1984).

[24] T. Tsuchida, H. Ujino, and M. Wadati, J. Phys. A **32**, 2239 (1999).

[25] M. J. Ablowitz, Y. Ohta, and A. D. Trubatch, Phys. Lett. A **253**, 287 (1999).

[26] V. S. Gerdjikov, M. I. Ivanov, and P. P. Kulish, J. Math. Phys. **25**, 25 (1984).

[27] A. A. Vakhnenko and Yu. B. Gaididei, Teor. Mat. Fiz. **68**, 350 (1986) [Theor. Math. Phys. **68**, 873 (1987)].

[28] O. O. Vakhnenko and V. O. Vakhnenko, Phys. Lett. A **196**, 307 (1995).

[29] G. B. Whitham, *Linear and Nonlinear Waves* (Wiley-Interscience, New York, 1974).

[30] C. Willis, M. El-Batanouny, and P. Stancioff, Phys. Rev. B **33**, 1904 (1986).

[31] H. J. Schnitzer, F. G. Mertens, and A. R. Bishop, Physica D **141**, 261 (2000).

[32] O. O. Vakhnenko, J. Phys. A **32**, 5735 (1999).

[33] O. O. Vakhnenko, Phys. Rev. E **60**, R2492 (1999).

[34] O. O. Vakhnenko and M. J. Velgakis, Phys. Rev. E **61**, 7110 (2000).

[35] A. B. Aceves, C. De Angelis, T. Peschel, R. Muschall, F. Lederer, S. Trillo, and S. Wabnitz, Phys. Rev. E **53**, 1172 (1996).

[36] V. V. Konotop, D. Cai, M. Salerno, A. R. Bishop, and N. Grønbech-Jensen, Phys. Rev. E **53**, 6476 (1996).

[37] K. Kundu, Phys. Rev. E **61**, 5839 (2000).

[38] F. Bloch, Z. Phys. **52**, 555 (1928).

[39] C. Zener, Proc. R. Soc. London, Ser. A **145**, 523 (1932).

[40] F. Löser, M. Sudzius, B. Rosam, V. G. Lyssenko, Y. Kosevich, M. M. Dignam, K. Köhler, and K. Leo, Physica E **7**, 285 (2000).
[41] M. Bruschi, D. Levi, and O. Ragnisco, Nuovo Cimento A **53**, 21 (1979).
[42] R. Scharf and A. R. Bishop, Phys. Rev. A **43**, 6535 (1991).
[43] V. V. Konotop, O. A. Chubykalo, and L. Vázquez, Phys. Rev. E **48**, 563 (1993).
[44] D. Cai, A. R. Bishop, N. Grønbech-Jensen, and M. Salerno, Phys. Rev. Lett. **74**, 1186 (1995).
[45] D. Cai, A. R. Bishop, N. Grønbech-Jensen, and M. Salerno, Phys. Rev. E **53**, 1202 (1996).
[46] R. Morandotti, U. Peschel, J. S. Aitchison, H. S. Eisenberg, and Y. Silberberg, Phys. Rev. Lett. **83**, 2726 (1999).
[47] G. Lenz, I. Talanina, and C. M. de Sterke, Phys. Rev. Lett. **83**, 963 (1999).
[48] H. L. F. Hemholtz, *On the Sensations of Tone as a Physiological Basis for the Theory of Music* (Dower, New York, 1954).
[49] Y. Kubota and T. Odagaki, Phys. Rev. E **61**, 3133 (2000).
[50] D. Anderson, Phys. Rev. A **27**, 3135 (1983).
[51] T. Ueda and L. Kath, Phys. Rev. A **42**, 563 (1990).
[52] P. L. Christiansen, Yu. B. Gaididei, M. Johansson, and K. Ø. Rasmussen, Phys. Rev. B **55**, 5759 (1997).
[53] Yu. S. Kivshar, A. M. Kosevich, and O. A. Chubykalo, Zh. Eksp. Teor. Fiz. **93**, 968 (1987) [Sov. Phys. JETP **66**, 545 (1987)].
[54] Yu. S. Kivshar, Zhang Fei, and L. Vázquez, Phys. Rev. Lett. **67**, 1177 (1991).
[55] O. O. Vakhnenko, Ukr. Fiz. Zh. **40**, 1021 (1995).